JOURNAL OF SPACECRAFT AND ROCKETS
Vol. 37, No. 1, January–February 2000

Simulations of Cold-Gas Nozzle and Plume Flows and Flight Data Comparisons

Nikos A. Gatsonis* and Richard A. Nanson†
Worcester Polytechnic Institute, Worcester, Massachusetts 01609
and
Gerald J. LeBeau‡
NASA Johnson Space Center, Houston, Texas 77058

The nozzle and plume flows of small cold-gas attitude control thrusters, plume interactions with spacecraft surfaces, and the induced pressure environment are investigated numerically. The motivation for this study originates from pressure measurements that exhibited nonperiodic pulses during the firings of small cold-gas thrusters onboard a suborbital spacecraft. Pitch, yaw, and roll cold-gas thrusters were located on the 0.56-m-diam base of the spacecraft. The conical spacecraft flew at altitudes between 670 and 1200 km and carried inside a pressure sensor connected to the side surface with a tube. Predictions of the pressure inside the sensor chamber are obtained using a semi-analytical model with inputs from coupled continuum and kinetic simulations. The nozzle and plume flows for each thruster are simulated using a three-dimensional Navier–Stokes solver until breakdown. Flowfield properties inside the breakdown surface are used as inputs to the direct simulation Monte Carlo calculations in a domain that includes the spacecraft geometry. Flowfield properties at the entrance of the sensor tube are used as inputs to an analytical model to obtain the pressure inside the sensor chamber. Simulations show plume expansion, reflection off the spacecraft surfaces, and backflow. Pressure predictions for the pitch and yaw thruster plumes that reach the sensor after expanding on the spacecraft base are in very good agreement with measurements. Pressure induced by the roll thrusters is shown to be very sensitive to their radial position at the Environmental Monitor Package base and decreases with decreasing radial distance. Pressure overprediction of the roll thrusters is attributed to possible difference between the simulated and actual radial position.

Nomenclature

C_m = most probable random speed at the pressure-sensor tube entrance, m/s
D_e = exit diameter of nozzle, mm
D_t = diameter of pressure-sensor tube, m
D_{th} = throat diameter of nozzle, mm
Kn = Knudsen number
L_t = length of pressure-sensor tube, m
M = Mach number
P = Bird's breakdown parameter
P_C = pressure inside pressure-sensor chamber, Pa
P_E = pressure at the entrance of the pressure-sensor tube, Pa
P_0 = stagnation pressure, kPa
Re = Reynolds number
S = ratio of mean speed to most probable random speed
T_C = temperature in the pressure-sensor chamber, K
T_E = temperature at the entrance of the pressure-sensor tube, K
T_w = wall temperature, K
T_0 = stagnation temperature, K
U_E = mean speed at the entrance of the pressure-sensor tube, m/s
x, y, z = coordinates used in the simulations
α_E = angle of attack at the entrance of the pressure-sensor tube, deg
β = polar angle of the pressure-sensor tube entrance, deg
λ = mean-free path, m
ν = collision frequency, s^{-1}
ρ = density of fluid, kg/m^3

Received 15 September 1998; revision received 7 May 1999; accepted for publication 14 May 1999.

*Assistant Professor, Computational Gas and Plasma Dynamics Laboratory, Mechanical Engineering Department, 100 Institute Road. Senior Member AIAA.

†Graduate Research Assistant, Computational Gas and Plasma Dynamics Laboratory, Mechanical Engineering Department, 100 Institute Road. Member AIAA.

‡Aerospace Engineer, Aeroscience and Flight Mechanics Division—EG3.

Introduction

PLUMES from attitude control thrusters contribute with their effluents to the induced environment about spacecraft. The study of plumes is important in predicting potentially adverse interactions of the induced environment with the spacecraft, its subsystems, and its sensors. There have been numerous ground-based experimental investigations of small thruster plumes.[1–5] Space-based experiments that demonstrated the effects of thruster plumes on the induced pressure environment include the Space Shuttle,[6] rocket experiments,[7] and Mir.[8] The interpretation of data collected onboard active spacecraft is often difficult because of the complexity of the induced environment, as well as because of the flow into such instruments that in many cases exhibits nonequilibrium and rarefaction effects.[9,10]

In this study we investigate the induced pressure environment because of firings of small cold-gas attitude control thrusters onboard the suborbital Environmental Monitor Package (EMP) spacecraft. The EMP carried a pressure sensor connected to the outside of the spacecraft with a long tube and recorded pressure spikes during the firings of its cold-gas thrusters. The details of the pressure-data analysis and interpretation are presented by Gatsonis et al.[11] In this paper we investigate the flow from the thruster nozzle to the plume and into the pressure sensor using an approach that combines continuum simulations, kinetic (rarefied gasdynamic) simulations, and a semi-analytical model. Numerical pressure predictions inside the sensor chamber are compared with EMP measurements. In a previous study using the direct simulation Monte Carlo (DSMC) method, we examined the response of the pressure sensor during the quiet-thruster period of the mission while the EMP was at altitudes from 560 km to reentry at 130 km (Ref. 10). It was determined that recorded pressure oscillations were because of ram-wake effects of the freestream and that the flow into the pressure-sensor tube exhibits three-dimensional and nonequilibrium effects. In the current effort we concentrate on the thruster-firing period of the mission

during which the EMP started from an altitude of 670 km, reached apogee at 1200 km and descended to 670 km.

Numerical simulation studies of nozzle and plume flows have been carried out traditionally with Navier–Stokes (N–S) codes.[12] The major failings of the continuous description of the expanding plume and often the nozzle flow itself are related to breakdown and nonequilibrium because of the rarefaction that are appropriately modeled by the DSMC method.[13–15] Recent studies have combined the two methods by following the flow via a N–S approach until breakdown is established, then continuing with a DSMC approach.[16–18] In this study, we apply a combined N–S/DSMC/semi-analytical approach. First, three-dimensional N–S simulations are performed in a domain that includes the nozzle and the EMP base until the breakdown surface of the continuum flow is established. Second, flowfield conditions from inside the breakdown surface are used as input to a three-dimensional DSMC code. Third, DSMC flowfield predictions at the entrance of the pressure-sensor tube are used as inputs to the model of Hughes and de Leeuw[19] and estimates of the pressure inside the sensor chamber are obtained. These predictions are then compared with the pressure data taken onboard EMP and issues related to the breakdown of the continuous flow, plume backflow, and plume impingement are discussed.

EMP Description and Problem Definition

The EMP payload was part of an experiment conducted by the Applied Physics Laboratory and contained a suite of instruments designed to measure the induced environment around the suborbital spacecraft. An approximate schematic of the EMP spacecraft is shown in Fig. 1 and the mission profile is shown in Fig. 2. The EMP has a 0.56-m-base diameter and its length is 0.52 m. The spacecraft's attitude control system, shown in detail in Fig. 3,

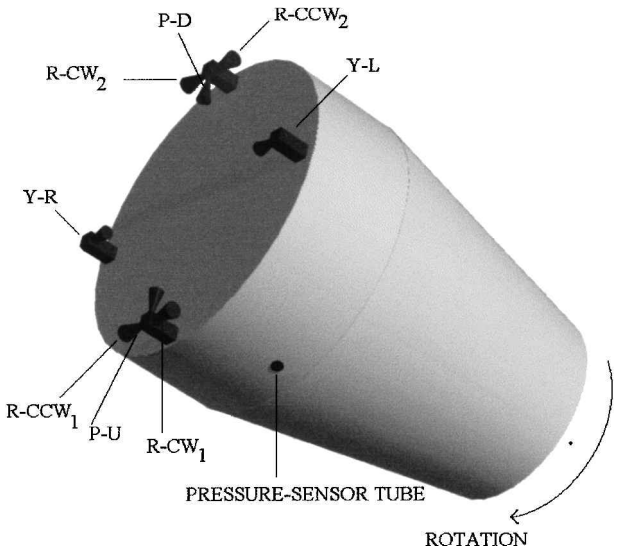

Fig. 1 EMP spacecraft showing the thrusters and the entrance to the pressure sensor.

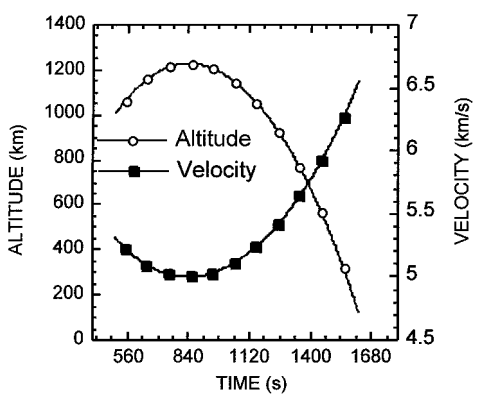

Fig. 2 Approximate EMP altitude and speed.

Table 1 EMP thruster characteristics

Thruster	Thrust, N	Exit diameter D_e, mm	Throat diameter D_t, mm
P-U, P-D	1.245	4.826	0.906
Y-R, Y-L	1.245	4.826	0.906
R-CW, R-CCW	3.278	5.588	1.6

Table 2 Reduced average pressure of individual thrusters

Thruster	Number of firings	Reduced average pressure, Pa	Standard deviation
P-D	27	3.19×10^{-5}	7.73×10^{-6}
P-U	210	1.3×10^{-4}	3.91×10^{-5}
Y-R	21	4.56×10^{-5}	1.34×10^{-5}
Y-L	1450	5.67×10^{-5}	2.04×10^{-5}
R-CW	270	2.09×10^{-4}	7.81×10^{-5}
R-CCW	248	1.41×10^{-5}	7.25×10^{-6}

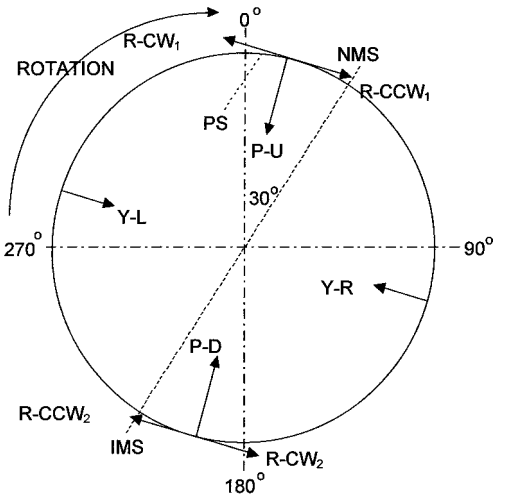

Fig. 3 EMP base showing the approximate thruster location (looking forward).

was mounted on its base and included eight N_2 cold-gas thrusters: pitch-down (P-D), pitch-up (P-U), yaw-right (Y-R), yaw-left (Y-L), two roll-clockwise (R-CC$_1$, R-CC$_2$), and two roll-counterclockwise (R-CCW$_1$, R-CCW$_2$). The nozzles were connected to solenoid valves and mounted on supports shown schematically in Figs. 1 and 3. The exact positions of the thrusters, the angular position of the pressure sensor, as well as the dimensions of the thruster-support system are only approximate. Nozzle characteristics are shown in Table 1. The EMP thruster-firing period covers the 500–1400-s (mission elapsed time) interval of the EMP mission. During this period the EMP ascended from 1000 km at 500 s, reached an apogee of 1230 km at 840 s, and then descended to 670 km at 1400 s as shown in Fig. 2. A cold-cathode ionization sensor monitored the neutral gas pressure about the spacecraft. The operating range of the sensor was from 4×10^{-5} to 0.1333 Pa ($\pm 15\%$) and pressure was sampled at 16.67 samples/s while the EMP was rotating with a period of approximately 10 s (frequency of 0.1 Hz). The pressure sensor itself was housed inside the spacecraft at a plane 0.15 m from the base of the spacecraft and was connected to the entrance hole on the surface by a tube with $L_t = 0.1$ m and $D_t = 0.022$ m. The pressure-sensor tube was located approximately 0.11 m off the axis as shown in Fig. 3. The analysis of the pressure-sensor response during the quiet-thruster period of the mission while the EMP was recording ram-wake oscillations was presented by Gatsonis et al.[10]

A typical pressure profile obtained during thruster firings is shown in Fig. 4 for the period between 840 and 850 s. The pressure spikes and the thruster firings coincide within the temporal resolution of the sampling as Fig. 4 shows. From the data it is evident that all thruster firings caused instantaneous pressure increases. A summary of the analysis of individual thruster effects by Gatsonis et al.[11] is shown in Table 2. To obtain the pressure associated with thruster firings,

the background pressure because of outgassing was subtracted from measurements and the result is designated as the reduced pressure. Table 2 suggests that thrusters of the same thrust levels did not produce similar pressure effects. For example, the R-CW thrusters produced almost one order of magnitude larger pressure amplitudes than the R-CCW. In contrast, differences between the yaw thrusters are small. As evident from Fig. 1 the EMP thruster plumes do not have a direct line of sight to the sensor entrance. Therefore, the induced pressure pulses must be produced by plume backflow and plume-surface interactions. It should be noted here that during the thruster-firing period the maximum ambient and incident pressure occurred at 670 km (1400 s) and are estimated to be approximately 3.7×10^{-8} and 1.7×10^{-6} Pa, respectively. These pressures are orders of magnitude lower than the recorded pressure inside the EMP sensor shown in Table 2. One can conclude that for this part of the EMP mission the effects of the ambient flow are negligible and all pressure measurements can be attributed to the thruster firings. Details of the data analysis can be found in Ref. 11.

Numerical Methodology

The EMP nozzle and plume flows are expected to exhibit features typical of small cold-gas thrusters. Estimates of the flow conditions, shown in Table 3, indicate that the EMP nozzle flows are expected to be well within the continuum regime. Near the nozzle lip the flow is expected to turn and undergo a rapid expansion reaching rarefaction quickly. Downstream within the plume a similar phenomenon is expected and a surface can be defined where rarefaction effects breakdown the continuous character of the flow. An estimate of the degree of rarefaction in a flow is given by Bird's breakdown parameter P (Ref. 13):

$$P = \frac{1}{\nu}\left|\frac{D(\ln \rho)}{Dt}\right| \tag{1}$$

It is commonly considered that the flow is in the transitional regime for $0.03 \leq P \leq 0.05$, in the rarefied regime for $P \geq 0.05$, and in the free-molecular regime for $P \geq 2$. In recent computational approaches for plumes that undergo transition, a N–S continuous solution is used to provide the approximate location of the breakdown surface that is subsequently used to provide input data for the rarefied calculations.[16–18] The methodology adapted in our study can be summarized as follows:

1) Perform three-dimensional N–S simulations of the nozzle and plume flow until breakdown using a domain that includes the thruster geometry and the necessary EMP surfaces.

Table 3 Estimates of flow conditions at the throat and exit of a thruster

	Throat		Exit	
Thruster	*Re*	*Kn*	*Re*	*Kn*
Yaw/pitch	635,000	1.75×10^{-6}	26,380	9.4×10^{-5}
Roll	736,000	1.51×10^{-6}	60,400	4.0×10^{-5}

2) Perform three-dimensional DSMC simulations for the plume flow in a domain that includes the EMP geometry up to the plane of the pressure sensor. The input surface to the DSMC is inside the breakdown surface as determined by the N–S simulations.

3) Use flow conditions at the entrance of the pressure-sensor tube and the theory of Hughes and de Leeuw[19] to obtain the pressure inside the sensor chamber.

Continuous Nozzle and Plume Flows

The continuous nozzle and plume solutions in this study are obtained using RAMPANT, a finite-volume code that solves the compressible N–S equations in arbitrary geometries.[20] Pitch and yaw thrusters are identical in size, have the same operating characteristics, and are firing toward the center of the EMP base as shown in Figs. 1 and 3. It is therefore sufficient to perform a N–S calculation that is characteristic of a pitch (or yaw) thruster to obtain the breakdown surface needed for the DSMC simulation. Such a three-dimensional simulation of nozzle and plume flows for a pitch (or yaw) thruster is performed using a computational domain shown in Fig. 5a. The exact radial distance of the pitch (or yaw) thruster is unknown and in our simulation it is placed at a radial distance of 0.28 from the center of the EMP base, i.e., on the perimeter, 0.0184 m above the surface, and is firing toward the X direction. The N–S domain contains the detailed geometry of the nozzle as shown in Fig. 5b. Preliminary simulations determined that breakdown in the plume of a pitch (or yaw) thruster occurs at a distance of approximately 0.2 m from the exit, much smaller than the 0.56-m diameter of the EMP base. Therefore, the entire EMP geometry was not included in the N–S simulations. Rather, the pitch (or yaw) domain contains a flat plate with dimension 0.2×0.15 m to represent part of the EMP base as Fig. 5a shows.

Three-dimensional N–S simulations using RAMPANT were also performed for the roll thrusters in a domain shown in Fig. 6a. Roll thrusters are located symmetrically on the EMP base and fire in pairs in antiparallel directions as shown in Fig. 3. The exact radial positions of the roll thrusters are unknown and in our simulations they are placed at a radial distance of 0.255 m from the center of the EMP base, i.e., 2.5 cm inside the perimeter, 0.0184 m above the surface as shown in Fig. 6a. Preliminary simulation of the plume flow of the roll thrusters showed that their effects are confined to only a portion of the EMP base. Therefore, during the R-CW firings, only the R-CW_1 thruster, located near the pressure sensor as shown in Figs. 1 and 3, is expected to contribute to the pressure inside the sensor. Similarly, during the R-CCW firings, only the R-CCW_1 thruster is expected to affect the pressure inside the sensor. Therefore, to simplify the computations only one roll thruster was included in the simulations assuming that the effects of the second thruster on the pressure inside the sensor are negligible.

The gas in all the N–S simulations is N_2 and the flow is modeled from the thruster throat, which is set as the inlet boundary with a stagnation pressure $P_0 = 1034$ kPa and stagnation temperature $T_0 = 300$ K. The outlet boundary is set to the ambient pressure at the altitude of the thruster firing and a temperature $T_w = 300$ K is used for all solid surfaces.

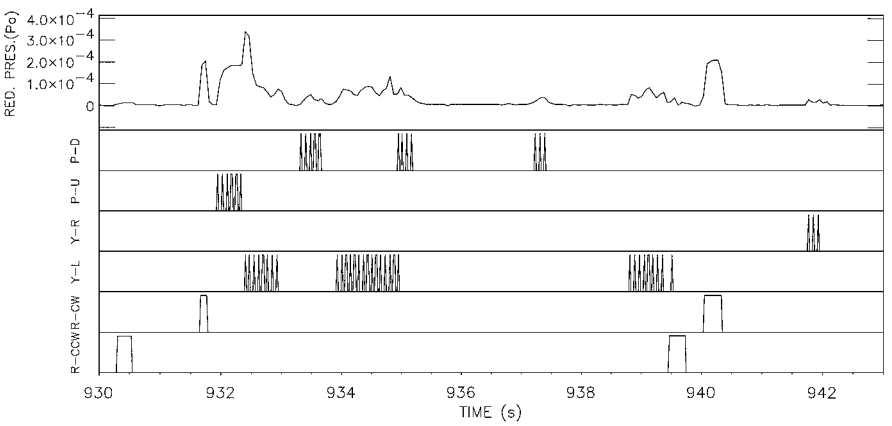

Fig. 4 Typical profile of EMP data showing the reduced pressure and thruster firings for the 840–850-s period.

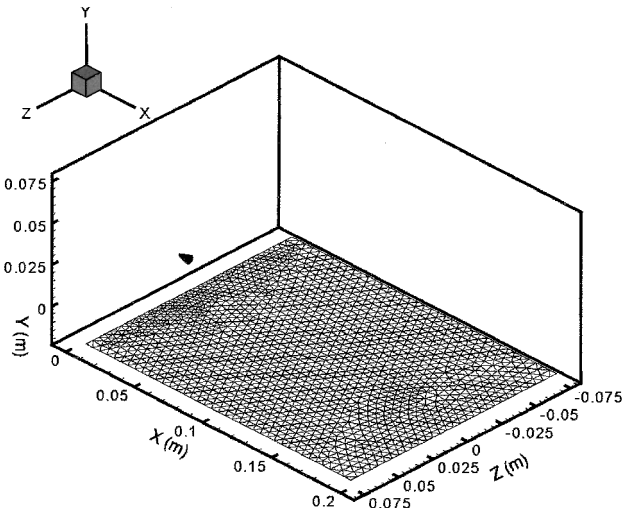

a)

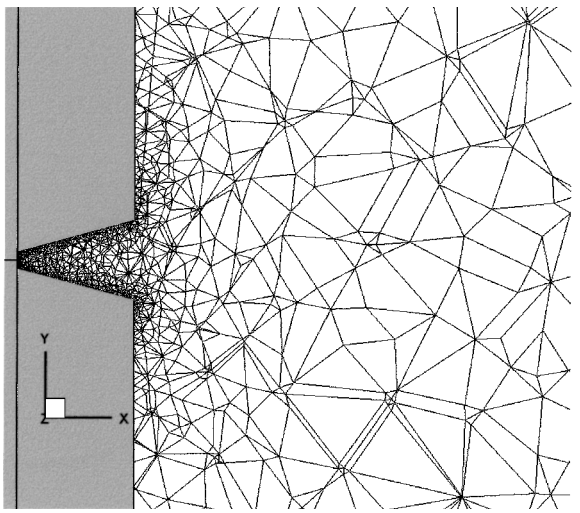

b)

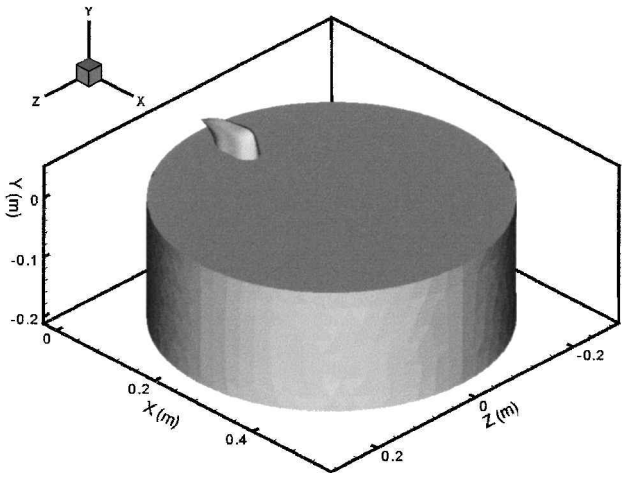

c)

Fig. 5 Computational domains used in the N–S and DSMC simulations for a pitch (or yaw) thruster. The thruster is located at ($x = 0, y = 0.0184, z = 0$) m and is firing toward the *X* direction. a) N–S computational domain for nozzle and plume flow. The EMP base is shown as a gridded region. b) Expanded view of the N–S grid showing the nozzle and near-exit area on the ($x, y, z = 0$)-m plane. c) DSMC computational domain showing the EMP surface and the DSMC input surface obtained from the N–S simulations.

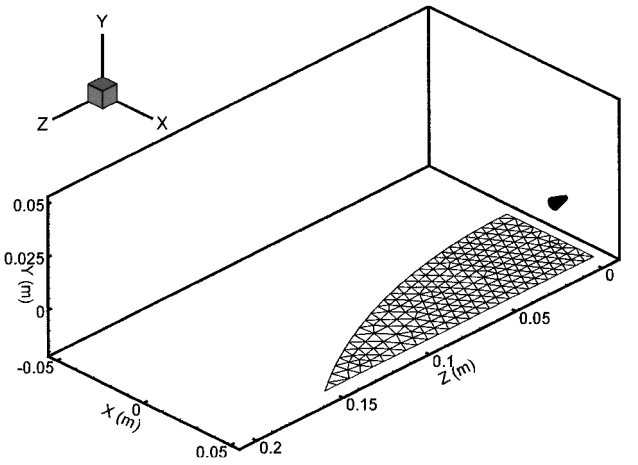

a)

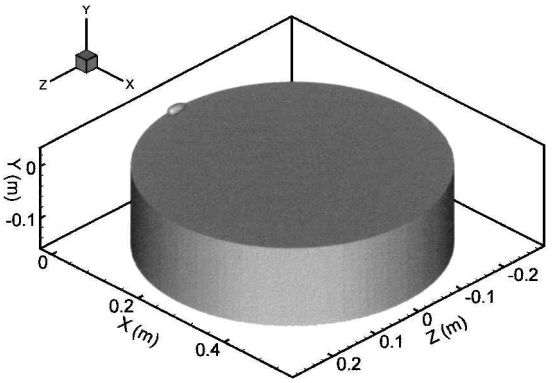

b)

Fig. 6 Computational domains used for the roll nozzle and plume flow. The roll thruster is located at ($x = 0.025, y = 0.0184, z = 0$) m and is firing toward the *Z* direction. a) N–S computational domain for nozzle and plume flow. The EMP base is shown as a shaded region. b) DSMC computational domain showing the EMP surface and the DSMC input surface obtained from the N–S simulations.

Rarefied Plume Flow

Modeling of the rarefied portion of the EMP plume flow is accomplished using a digital-to-analog converter, a three-dimensional DSMC code developed at the NASA Johnson Space Flight Center.[21,22] The code uses an unstructured triangular grid for surface representation, which is embedded in a two-level Cartesian flowfield grid that provides a grid adaptation capability. The domains used in the DSMC simulations include the EMP spacecraft up to the plane of the pressure sensor. Figure 5c shows the DSMC domain for a pitch (or yaw) plume and Fig. 6b for a roll plume. The DSMC input surface for the pitch (or yaw) plume, shown in Fig. 5c, is located inside the breakdown region of the plume defined as the isosurface of $P \approx 0.03$ from the N–S simulations. The DSMC input surface for the roll plume was placed well within the breakdown surface as shown in Fig. 6b. The input data necessary for the DSMC simulation are taken from the N–S simulations using a linear interpolation scheme and the TecPlot visualization software.[23] The boundaries of the computational domain are set as the ambient freestream conditions. The EMP surface is set to a diffuse reflection and temperature $T_w = 300$ K based on measurements obtained onboard the EMP.

The cells of the surface grid are sized so as to represent the geometry or capture the pertinent flowfield features of the inflow for the breakdown surface adequately. The interior grid is initially discretized by a uniform Cartesian grid and a subsequent DSMC simulation is performed. Based on this initial solution, the flowfield grid is refined such that the local cell size corresponds to the new flow conditions. Once the grid is adapted sufficiently, the solution can be allowed to run until it reaches steady state. It was determined for the EMP thrusters that the time of thruster operation is larger than the time required for the plume to reach steady state. The EMP thrusters fired with impulses that lasted for 0.03 s each with multiple pulses

per firing. It is also demonstrated in Fig. 4, as well as by Gatsonis et al.,[11] that pressure spikes occurred simultaneously with the firings followed by a gradual decay. All of the preceding suggests that steady-state DSMC results should be sufficient to predict the flow conditions at the entrance of the pressure-sensortube. In a case where predictions of the pressure evolution were sought, unsteady DSMC calculation would be required.

Results and Discussion

Pitch and Yaw Thrusters

Pitch and yaw thrusters are identical in size and fire directly in the middle of the EMP base as Fig. 5a shows. We therefore examine the flow characteristics of a typical case that can be considered as representative of the flow resulting from a pitch (or yaw) thruster. Number density, temperature, and Mach contours from the N–S simulation for a pitch (or yaw) thruster are presented in Figs. 7a, 7b, and 7c, respectively. The results are plotted on the $(x, y, z = 0)$-m plane passing through the nozzle centerline perpendicular to the EMP base. Figures 7a–7c (left) show an expanded view of the flowfield covering the nozzle and the near-exit region while Figs. 7a–7c (right) show the plane covering the entire computational domain. The flow is shown to accelerate from the throat and reaches $M \approx 5$ close to the exit. Figure 7 also exhibits the rapid expansion that occurs near the nozzle lip and the formation of a relatively thin boundary layer inside the nozzle. The near-sonic Mach contours shown in Fig. 7c (left) emanate from the thruster throat and terminate at the nozzle lip. The flow shown in Fig. 7 (right) expands in the plume region and its temperature and density drop significantly. At a distance of 0.2-m downstream the exit the density is 10^{21} m^{-3}, almost three orders of magnitude lower than the thruster exit. Figure 7 (right) shows the interaction of a pitch (or yaw) plume with the EMP base and the formation of a reflecting wave. Figure 8 depicts the contours of P. The noticeable feature is that transitional flow does not begin until at least 0.2-m downstream the nozzle exit. The breakdown surface is asymmetric in the Y direction because of the plume-surface interaction.

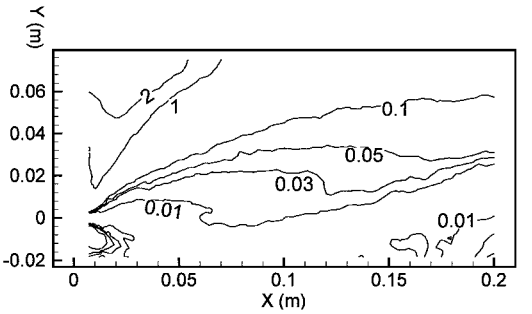

Fig. 8 Breakdown parameter contours for a pitch (or yaw) thruster plume from N–S simulation on the $(x, y, z = 0)$-m plane.

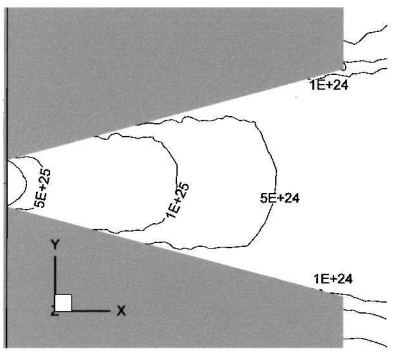

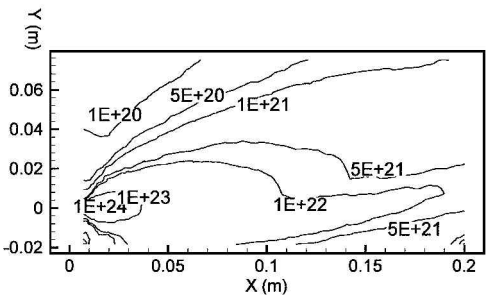

a) Number density contours (m^{-3})

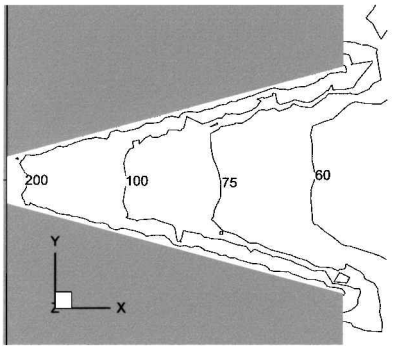

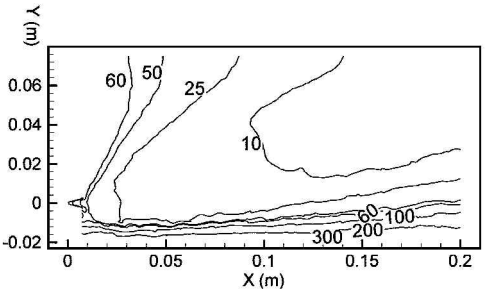

b) Temperature contours (K)

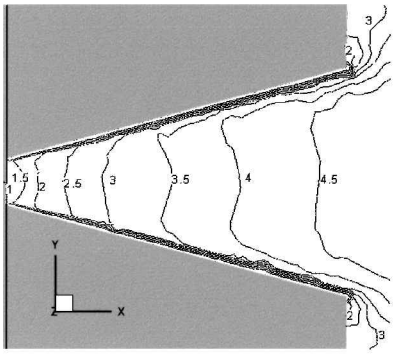

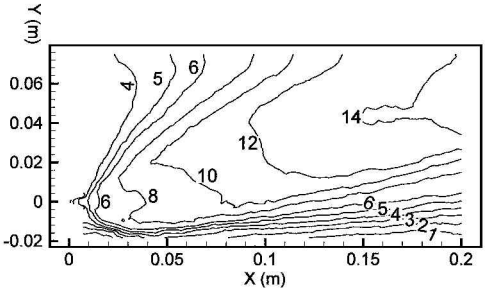

c) Mach contours

Fig. 7 Pitch (yaw) nozzle and plume flowfield from N–S simulations on the $(x, y, z = 0)$-m plane: left, expanded view of the nozzle and near-exit flow region, and right, entire domain.

Number density predictions from the DSMC simulation for a pitch (or yaw) thruster are shown in Fig. 9a. Figure 9b shows the $(x, y, z = 0)$-m plane that passes through the centerline of the nozzle and is perpendicular to the EMP base. Figure 9c depicts the thruster plane $(x, y = 0.0184, z)$ m passing though the nozzle centerline parallel to the EMP base and Fig. 9d depicts the $(x, y = -0.15, z)$-m pressure-sensor plane parallel to the EMP base. The plume flow can be seen in Fig. 9b reflecting off the surface of the spacecraft. Another feature of the plume flow depicted in Fig. 9b is the expansion around the spacecraft edge at the far side of the thruster, as well as the backflow behind the thruster. The density at the parallel thruster plane of Fig. 9c is symmetric because of the firing orientation of the pitch (or yaw) thruster. On the pressure-sensor plane shown in Fig. 9d the density decreases close to the surface of the EMP and is higher in the backflow region of the thruster.

Figures 10a and 10b present the EMP surface pressure predicted by DSMC. Two views are provided so that the entire pressure field over the EMP can be seen. The pressure is highest at the base of the spacecraft where the plume impinges and gets reflected. However, as the plume flow moves over the edge of the EMP base and down to its sides, the pressure drops rapidly. Figure 10b shows the pressure contours in the backflow region of the thruster and demonstrates the increase in surface pressure because of pitch (or yaw) plume backflow.

Roll Thrusters

The roll thrusters are larger than the pitch and yaw and fire in the Z direction away from the EMP base as shown in Fig. 6a. Number density, temperature, and Mach from the N–S simulation are presented in Fig. 11. The results are plotted on the $(x = 0, y, z)$-m

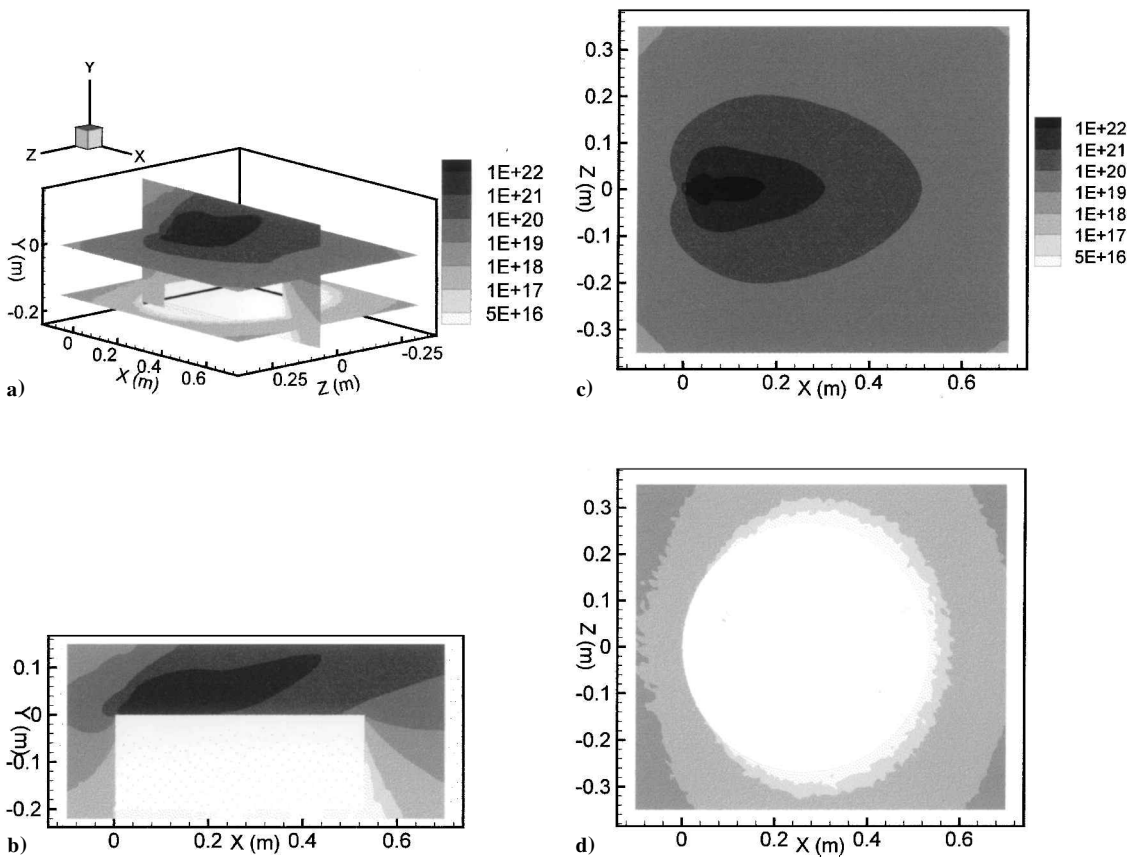

Fig. 9 DSMC number density (m^{-3}) for a pitch (or yaw) thruster plume. The thruster is located at ($x = 0, y = 0.0184, z = 0$) m and is firing in the X direction. a) Three-dimensional view. b) Perpendicular thruster plane ($x, y, z = 0$) m. c) Parallel thruster plane ($x, y = 0.0184, z$) m. d) Pressure sensor plane ($x, y = -0.15, z$) m.

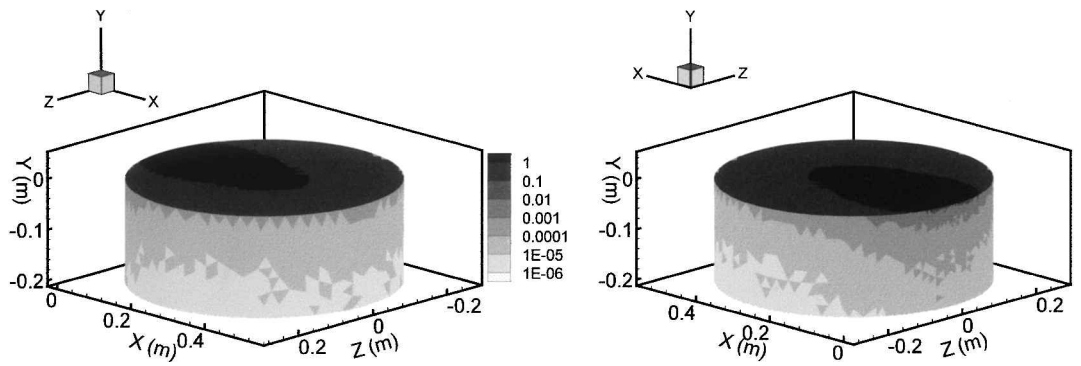

a) Downstream region **b) Backflow region**

Fig. 10 DSMC surface pressure (Pa) for a pitch (or yaw) thruster plume. The thruster is located at ($x = 0, y = 0.0184, z = 0$) m and is firing toward the X direction.

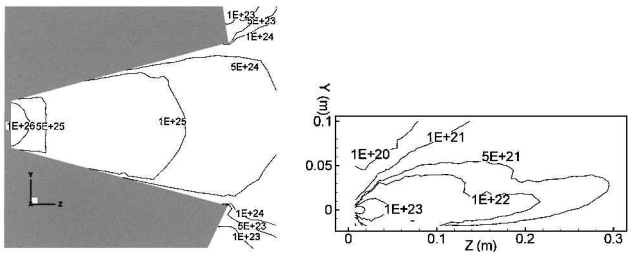

a) Number density contours (m^{-3})

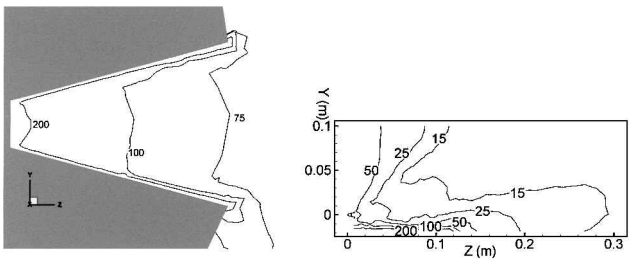

b) Temperature contours (K)

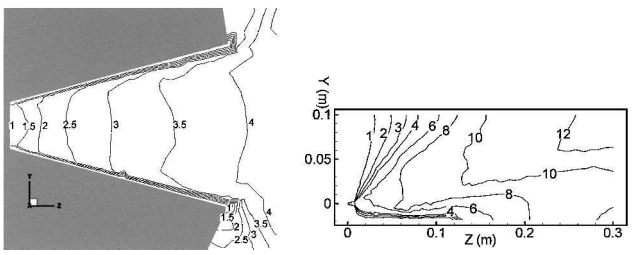

c) Mach contours

Fig. 11 Roll nozzle and plume flowfield from N–S simulations on the $(x, y, z = 0)$-m plane: left, expanded view of the nozzle and near-exit region, and right, entire domain.

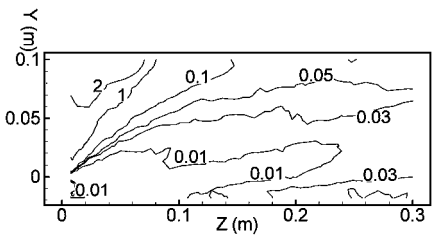

Fig. 12 Breakdown parameter for a roll thruster plume from N–S simulations shown on the $(x, y, z = 0)$-m plane.

plane passing through the nozzle centerline perpendicular to the EMP base. Figure 11 (left) shows the expanded view of the flowfield within the nozzle and the near-exit region while Fig. 11 (right) shows the entire plane of the computational domain. The characteristics inside the nozzle are similar to those of the pitch (and yaw) thrusters. However, because of the partial reflection of the roll plume off the EMP base, the plume region characteristics are different from those of the pitch (and yaw) thrusters. The plume shown in Fig. 11 (right) expands and its temperature and density drop significantly. At a distance of 0.2-m downstream of the thruster exit, the density is approximately 10^{22} m^{-3}, almost three orders of magnitude lower than that at the thruster exit. Figures 11a–11c (right) show that the interaction of the plume with the EMP base results in the formation of a reflecting wave that is weaker than that of the pitch (and yaw) case. Figure 12 depicts the contours of P. The noticeable feature is that transitional flow does not begin until at least 0.2 m downstream of the exit and the breakdown surface is not symmetric because of the plume-surface interaction.

Figure 13 shows DSMC number density predictions for a roll thruster. Figure 13b shows the $(x = 0.025, y, z)$-m plane that passes through the centerline of the nozzle and is perpendicular to the EMP base. Figure 13c depicts the parallel thruster plane $(x, y = 0.0184, z)$ m and Fig. 13d depicts the $(x, y = -0.15, z)$-m pressure-sensor plane parallel to the EMP base. The plume is shown in Fig. 13b to reflect off the surface of the spacecraft and to form a large backflow region. The density at the parallel thruster plane in Fig. 13c is asymmetric because of the firing of the roll thruster close to the perimeter of the EMP base. The pressure-sensor plane in Fig. 13d shows that the density perturbation is confined to the roll-thruster side of the EMP as expected.

Figures 14a and 14b present the EMP surface-pressure predicted by DSMC. Pressure is higher on the EMP base that is closer to the roll thruster. Also, the part of the roll plume flow closer to the perimeter creates the high surface pressure levels shown in Fig. 14a. At the side opposite to the roll thruster, the pressure is at background levels. This is consistent with our assumption that, although the roll thrusters fire in pairs, they are not expected to contribute equally to the EMP surface pressure.

Data Comparison

Although the coupled N–S/DSMC simulations of the nozzle and plume flows provide the flow conditions at the surface of the EMP and therefore the entrance of the pressure-sensor tube, some means of estimating the pressure inside the sensor chamber are needed to compare with the measurements. In our previous analysis of the quiet-thruster period we focused on the response of the pressure sensor and its connecting tube to the incoming flow using DSMC.[10] It was shown that the flow into the sensor tube exhibits significant rarefaction and nonequilibration. Both angle of attack and the EMP geometry were found to have profound effects on the equilibration process inside the tube and sensor chamber.[10] In the current study we use the theory of Hughes and de Leeuw[19] to estimate the pressure inside the pressure-sensor chamber as it was deemed unnecessary to perform DSMC simulation for the internal tube flow.

A schematic of the underlying EMP pressure-sensor geometry used for the application of the pressure-probe theory of Hughes and de Leeuw is shown in Fig. 15. Our coupled N–S/DSMC simulations showed that the plume near the entrance of the pressure-sensor tube is in a rarefied state and the flow velocity is almost parallel to the EMP side surface. A tube with a ratio $D = 0.22$ connects the sensor chamber with the external plume flow incoming at α_E, U_E, T_E, and $P_E = n_E k T_E$ under equilibrium conditions. The flow conditions in the sensor chamber are designated by T_C and the equilibrated pressure inside the volume, $P_C = n_C k T_C$, is presented in terms of the pressure ratio $R(S_E, D, \alpha_E)$ by

$$(P_C/P_E)(T_E/T_C)^{\frac{1}{2}} = R(S_E, D, \alpha_E) \tag{2}$$

The expression for $R(S_E, D, \alpha_E)$ contains integrals of the incoming drifting Maxwellian distribution function that can be performed numerically[19] and is a function of $S_E = U_E/C_{mE}$, where $C_{mE} = \sqrt{(2kT_E/m_E)}$. At equilibrium the flux of molecules that exit the chamber is equal to the flux entering the tube. This model was implemented in a computer code[24] and used in our analysis with input conditions at the pressure-sensor tube entrance obtained from the N–S/DSMC simulations. A velocity transformation is needed to obtain U_E and α_E with respect to the tube axis from the DSMC velocities that are given in terms of the XYZ coordinate system located at the thruster. Insight on this transformation can be gained from Fig. 16 that displays the geometry of each EMP thruster and the projection of the EMP base onto the pressure-sensor plane. In Fig. 16 the entrance to the pressure-sensor tube is designated by E and is at an angle β with the X axis, while the centerline of the pressure-sensor tube is oriented at an angle γ with the radius OE. The velocity and pressure inputs needed for the Hughes and de Leeuw model are shown in Table 4. The equilibrated chamber temperature is assumed to be $T_C = 300$ K and the predictions of P_C are shown in Table 4.

A comparison between the sensor-chamber pressure predictions and the EMP reduced average pressure is shown in Fig. 17. The chamber pressures predicted for the pitch and yaw thrusters are very close to the measurements. The flux at the entrance of the pressure-sensor tube is mainly because of the thermal component of the plume

Table 4 Flow conditions at the entrance of the sensor tube used as inputs to the semi-analytical model of Hughes and deLeeuv for predictions of the sensor-chamber pressure P_C

Thruster	N_E, m^{-3}	T_E, K	U_E, m/s	α_E, deg	P_E, Pa	P_C, Pa
P-D	2.07×10^{16}	119	311	89	3.38×10^{-5}	3.8×10^{-5}
P-U	1.20×10^{17}	115	336	90	1.91×10^{-4}	1.98×10^{-4}
Y-R	1.97×10^{16}	87	297	86	2.35×10^{-5}	3.43×10^{-5}
Y-L	2.05×10^{16}	112	246	90	3.16×10^{-5}	3.62×10^{-5}
R-CW_1	1.47×10^{18}	81	571	95	1.64×10^{-3}	1.92×10^{-3}
R-CCW_1	4.78×10^{17}	79	493	81	5.12×10^{-4}	6.33×10^{-4}

velocity, and nonequilibrium effects do not seem to play a significant role. These effects, if present, could be resolved with DSMC computations that cover the flow inside the pressure tube and sensor. In contrast, in our analysis of the response of the pressure sensor during the ram-wake period of the mission, it was identified that the Hughes and de Leeuw theory was unable to predict the nonzero angle-of-attack cases because of EMP surface geometrical effects.[10] It should be noted that these nonequilibrium effects were identified while the EMP was flying in the denser part of the thermosphere at altitudes below 560 km.

Figure 17 shows that our roll simulations overpredict both the R-CW_1 and R-CCW_1 chamber pressures. As we described earlier,

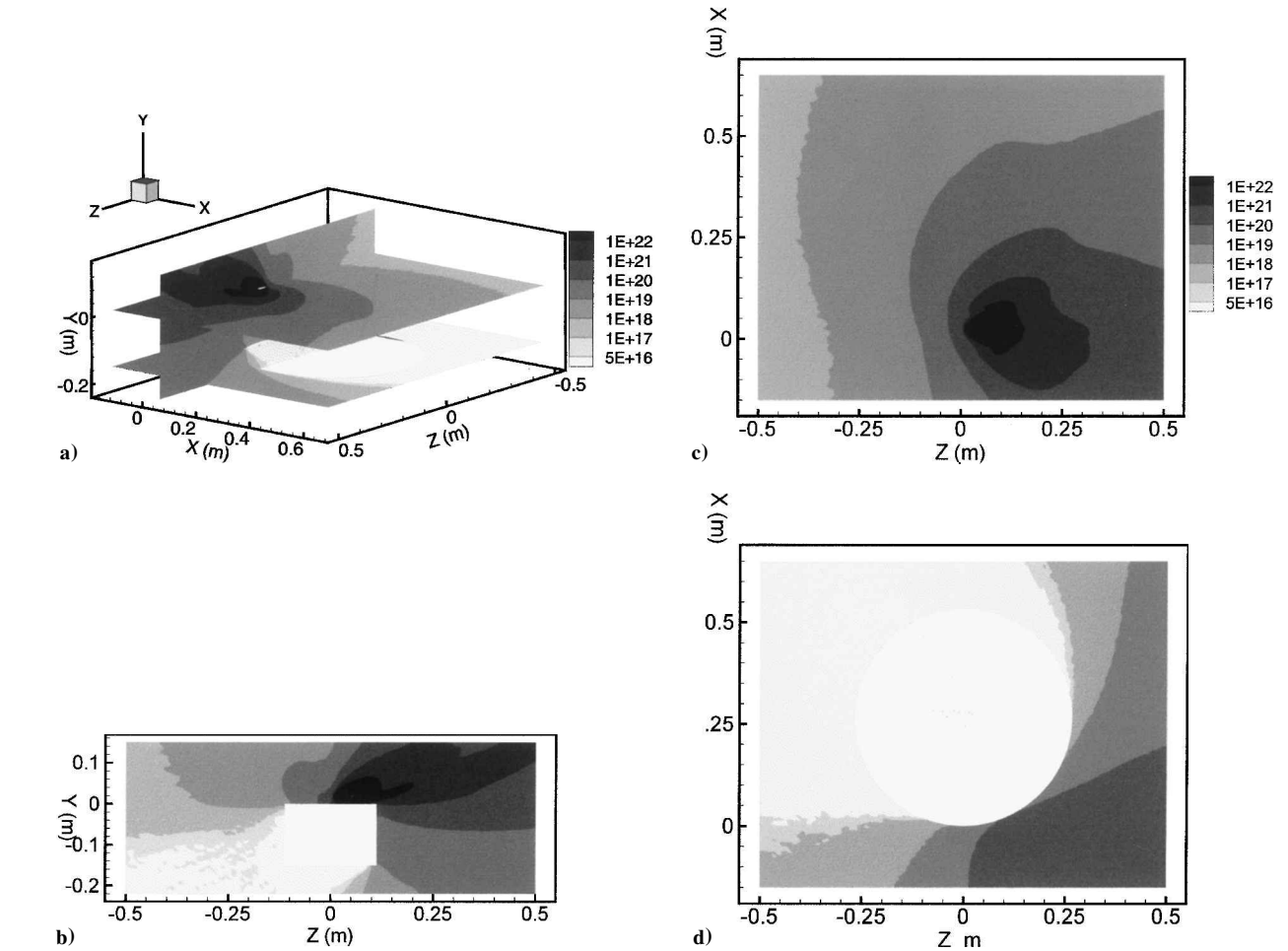

Fig. 13 DSMC number density (m^{-3}) for a roll thruster plume. The thruster is located at ($x = 0.025, y = 0.0184, z = 0$) m and is firing in the Z direction. a) Three-dimensional view. b) Perpendicular thruster plane ($x = 0.025, y, z$) m. c) Parallel thruster plane ($x, y = 0.0184, z$) m. d) Pressure sensor plane ($x, y = -0.15, z$) m.

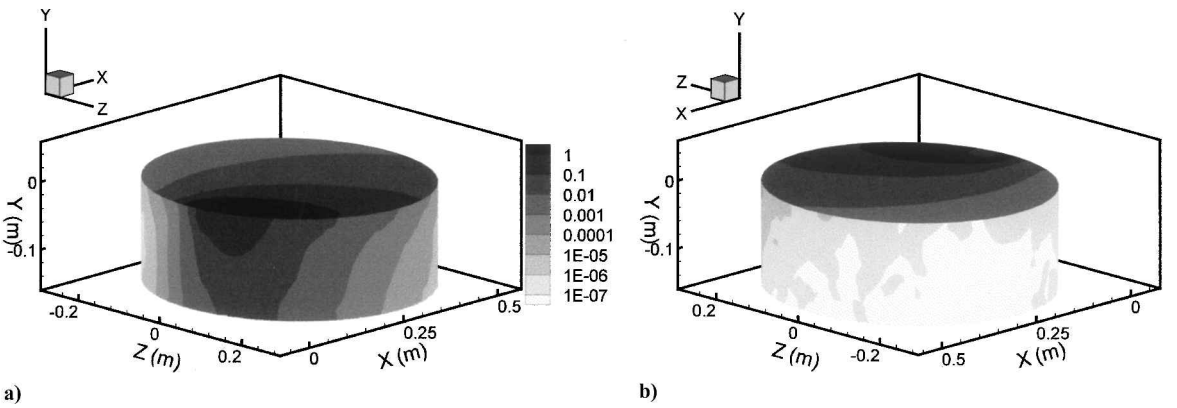

Fig. 14 DSMC surface pressure (Pa) for a roll thruster plume. The thruster is located at ($x = 0.025, y = 0.0184, z = 0$) m and is firing in the Z direction. a) Roll thruster side. b) Opposite to the roll thruster side.

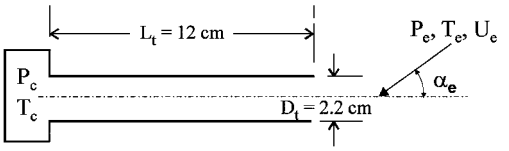

Fig. 15 Schematic of the EMP pressure sensor.

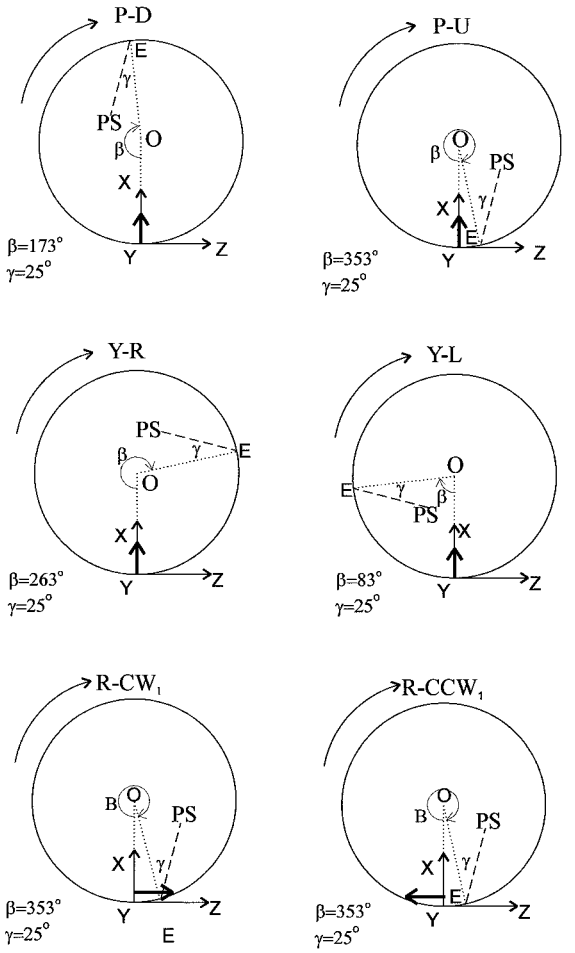

Fig. 16 Pressure-sensor plane showing the orientation of the pressure-sensor tube and the projection of the *XYZ* coordinate system used in the DSMC simulations. The thruster firing direction is designated with the bold vector.

the exact radial position, the size of the solenoid valve, and the mounting support shown in Fig. 3 are unknown. In the simulations the roll thrusters were placed at a radial position of 0.255 m from the center of the EMP base, i.e., 2.5 cm inside the perimeter. This thruster position, shown also in Fig. 16, allows the R-CW$_1$ plume and the R-CCW$_1$ backflow to undergo expansion on a portion of the EMP base before reaching the pressure-sensor entrance. That expansion reduces the flux to the sensor tube and, consequently, the pressure inside the sensor chamber but not as much as observed during the flight experiment as Fig. 17 clearly shows. To examine the effects of the position of the roll thruster on the sensor chamber pressure, we performed an additional simulation placing the roll thrusters at a radial position of 0.28 m, i.e., at the perimeter of the EMP base. In this case a major part of the R-CW$_1$ plume and the R-CCW$_1$ backflow can reach directly the entrance of the pressure-sensor tube and results in two to three order of magnitude larger chamber-pressures compared with measurements. These simulation results are designated as Roll Case 2 in Fig. 17. This analysis demonstrates the drastic effect of the roll thruster position on the predicted pressure: in the simulations as the thruster is moved inward from the perimeter, the plume undergoes expansion over a larger part of the EMP base, thus reducing the induced sensor-pressure. In contrast to the roll, plumes from P-D, Y-R, and Y-L thrusters expand

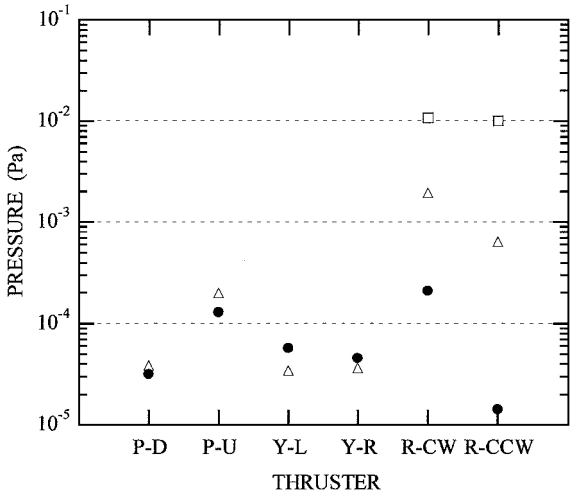

Fig. 17 Comparison between EMP reduced average pressure (Pa) from measurements and predicted sensor-chamber pressure (Pa): ●, EMP reduced average pressure; △, predicted sensor-chamber pressure; and □, predicted sensor-chamber pressure-roll case 2.

over the entire EMP base of 0.56 m before reaching the entrance to the pressure sensor and are insensitive to any small variation in the radial position of these thrusters. Similar arguments can be made for the backflow of the P-U thruster. Therefore, despite the possible difference between simulation and actual radial position of the pitch and yaw thrusters, predictions are very close to the data. One important conclusion from our simulations is that in certain cases, because of the nature of plume/surface interactions, the detailed position of thrusters must be known to obtain accurate predictions.

Conclusions

In this study we investigated the nozzle and plume flow of small cold-gas attitude control thrusters, plume interactions with spacecraft surfaces and the induced pressure environment. In addition, we investigated the response of a pressure sensor onboard a small spacecraft during thruster firings. The preceding issues are important in the interpretation of data taken onboard active spacecraft, as well as in the determination of plume/spacecraft interactions.

The pressure data used in this study were taken onboard the EMP, a small suborbital spacecraft during the thruster-firing period of the mission with the spacecraft flying from 670 km to apogee at 1230 km and down to 670 km. A pressure sensor onboard the EMP was housed inside the spacecraft on a plane 0.15 m below its base and was connected to the outside surface with a 0.1-m-long, 0.022-m-diam tube. Measurements showed that pressure pulses appeared instantaneously with the firings even for thrusters without a direct line of sight with the sensor entrance.

Numerical simulations of the nozzle and plume flows were performed using a combination of continuum and kinetic approaches. Predictions of the sensor-chamber pressure were based on a semi-analytical approach. For each EMP thruster, the nozzle and plume flow was followed until breakdown using a three-dimensional N–S code in a domain that included the detailed geometry of the nozzle and the EMP base. Data from inside the breakdown surface were interpolated and used as input to a three-dimensional DSMC plume simulation. The DSMC domain included the EMP spacecraft geometry beyond the plane of the pressure sensor. The coupled N–S/DSMC flowfield predictions at the entrance of the pressure-sensor tube were then used as inputs to the Hughes and de Leeuw model to obtain the pressure inside the sensor chamber. The N–S and DSMC simulations showed the complex structure of the plumes as they expanded over the EMP surfaces, as well as plume reflection and backflow. Chamber pressure predictions were compared with measurements. It was shown that the pressure predictions for the pitch and yaw thrusters were very close to the EMP measurements. The plumes of the P-D, Y-R, and Y-L thrusters and the backflow of the P-U thruster reached the pressure-sensor entrance after expanding on the EMP base over a distance of approximately 0.56 m.

Therefore, any possible difference between simulation and actual radial position of the pitch and yaw thrusters did not affect the flow conditions at the pressure-sensor entrance. Chamber pressure predictions for the roll thruster were larger than the EMP measurements by almost an order of magnitude. The roll thrusters were placed at a radial distance of 0.255 m from the EMP center in our simulations. As a result, the R-CW_1 plume and the R-CCW_1 backflow reached the entrance of the pressure-sensor after expanding on a small portion of the EMP base. Simulations with the roll thrusters located on the EMP perimeter at radial position of 0.28 m resulted in overprediction by two orders of magnitude for the R-CW_1 and three orders for the R-CCW_1. This overprediction was because of direct flow of the R-CW_1 plume and the R-CCW_1 backflow into the entrance of the pressure sensor. Most likely the roll thrusters were located on the EMP base in a position that allowed expansion of their plume or their backflow over a larger part of the EMP surface compared to that in the simulations. An important conclusion from these simulations is that in certain cases, as for example the roll thrusters, knowledge of the exact thruster configuration is necessary to obtain accurate flow predictions.

Overall the combination of advanced numerical techniques and a semi-analytical model is shown to be a very valuable predictive tool. Coupling of continuum and kinetic (rarefied gasdynamic) approaches can provide predictions of complex expanding plume flows and their interactions with surfaces. Relatively simple and computationally inexpensive semi-analytical models, such as the Hughes and de Leeuw, are also capable of providing accurate predictions. When applying such semi-analytical tools, care should be taken in examining that flow conditions meet the theoretical assumptions, as nonequilibrium effects cannot be ruled out entirely.

References

[1]Rothe, D. E., "Experimental Study of Viscous Low-Density Nozzle Flow," Cornell Aeronautical Lab., Inc., AI-2590-A-2, Buffalo, NY, 1970.

[2]Dettleff, G., Boettcher, R. D., Dankert, C., Koppenwallner, G., and Legge, H., "Attitude Control Thruster Plume Flow Modeling and Experiments," *Journal of Spacecraft and Rockets*, Vol. 23, No. 5, 1985, pp. 476–481.

[3]Legge, H., and Dettleff, G., "Pitot Pressure and Heat Transfer Measurements in Hydrazine Thruster Plumes," *Journal of Spacecraft and Rockets*, Vol. 23, No. 4, 1986, pp. 357–362.

[4]Boyd, I. D., Penko, P. F., Meissner, D. L., and DeWitt, K. J., "Experimental Investigations of Low Density Nozzle and Plume Flows of Nitrogen," *AIAA Journal*, Vol. 30, No. 10, 1992, pp. 2453–2461.

[5]Dettleff, G., and Plahn, K., "Experimental Investigation of Fully Expanded Free Jets and Plumes," 21st International Symposium on Rarefied Gas Dynamics, Marseilles, France, 1998.

[6]Wolf, E., and Von Zahn, U., "The Shuttle Environment: Effects of Thruster Firings on Gas Density and Composition in the Payload Bay," *Journal of Geophysical Research—Space Physics*, Vol. 91, No. A3, 1986, pp. 3270–3278.

[7]Pickett, J. S., Morgan, D. D., and Merlino, R. L., "Payload Environment and Gas Release Effects on Sounding Rocket Neutral Pressure Measurements," *Journal of Spacecraft and Rockets*, Vol. 33, No. 4, 1996, pp. 501–506.

[8]Ivanov, M. S., Markelov, G. N., Gerasimov, Yu. I., Krylov, A. N., Mishina, L. V., and Sokolov, E. I., "Free-Flight Experiment and Numerical Simulation for Cold Thruster Plume," AIAA Paper 98-0898, Jan. 1998.

[9]Moss, J. N., and Bird, G. A., "Monte Carlo Simulations in Support of the Shuttle Upper Atmospheric Mass Spectrometer Experiment," *Journal of Thermophysics*, Vol. 2, No. 2, 1988, pp. 138–144.

[10]Gatsonis, N. A., Maynard, E., and Erlandson, R. E., "Monte Carlo Modeling and Analysis of Pressure Sensor Measurements During Suborbital Flight," *Journal of Spacecraft and Rockets*, Vol. 34, No. 1, 1997, pp. 83–91.

[11]Gatsonis, N. A., Erlandson, R. E., Swaminathan, P. K., and Kumar, C. K., "Analysis of Pressure Measurements During Cold-Gas Thruster Firings Onboard Suborbital Spacecraft," *Journal of Spacecraft and Rockets*, Vol. 36, No. 5, 1999, pp. 688–692.

[12]Gilmore, M. R., Gallis, M. A., and Harvey, J. K., "Breakdown of Continuum Solvers in Rapidly Expanding Flows," AIAA Paper 95-2134, June 1995.

[13]Bird, G. A., "Breakdown of Translational and Rotational Equilibrium in Gaseous Expansions," *AIAA Journal*, Vol. 8, No. 11, 1970, pp. 1998–2003.

[14]Bird, G. A., "Breakdown of Continuum Flow in Freejets and Rocket Plumes," *Rarefied Gas Dynamics*, edited by S. S. Fisher, AIAA, New York, 1980, pp. 681–694.

[15]Bird, G. A., *Molecular Gas Dynamics and the Direct Simulation of Gas Flows*, Clarendon, Oxford, 1994.

[16]Rault, D. F. G., "Methodology for Thruster Plume Simulation and Impingement Effects Characterized Using DSMC," AIAA Paper 95-2032, June 1995.

[17]Lumpkin, F. E., III, Le Beau, G. J., and Stuart, P. C., "Enhanced Analysis of Plume Impingement During Shuttle-Mir Docking Using a Combined CFD and DSMC Methodology," AIAA Paper 96-1877, June 1996.

[18]Ivanov, M. S., Markelov, G. N., Kashkovsky, A. V., and Giordano, D., "Numerical Analysis of Thruster Plume Interaction Problems," *Proceedings of the 2nd European Space Propulsion Conference*, ESA, Noordwijk, The Netherlands, 1997, pp. 603–610.

[19]Hughes, P. C., and de Leeuw, J. H., "Theory for the Free Molecule Impact Probe at an Angle of Attack," *Rarefied Gas Dynamics*, Vol. 1, Academic, New York, 1965, pp. 653–676.

[20]Fluent Inc. Computational Fluid Dynamics Software, "Fluent/UNS & Rampant" Release 4.0, Lebanon, NH, April 1996.

[21]Wilmoth, R. G., LeBeau, G. J., and Carlson, A. B., "DSMC Grid Methodologies for Computing Low Density Hypersonic Flows About Reusable Launch Vehicles," AIAA Paper 96-1812, June 1996.

[22]LeBeau, G. J., "The DAC Series: Preprocessor—Run Code—Postprocessors," Revision 95v1, NASA Johnson Space Center, Houston, TX, 1997.

[23]"TecPlot," Amtec Engineering Inc., Ver. 7, Bellevue, WA, Aug. 1996.

[24]Maynard, E., "Direct Simulation Monte Carlo Analysis of Rarefied Gas Flows in Tubes," M.S. Thesis, Worcester Polytechnic Inst., Worcester, MA, April 1996.

R. G. Wilmoth
Associate Editor